

Electrical Control of Exchange Bias Mediated by Graphene

Y. G. Semenov, J. M. Zavada, and K. W. Kim

Department of Electrical and Computer Engineering,
North Carolina State University, Raleigh, NC 27695-7911

Abstract

The role of graphene in mediating the exchange interaction is theoretically investigated when it is placed between two ferromagnetic dielectric materials. The calculation based on a tight-binding model illustrates that the magnetic interactions at the interfaces affect not only the graphene band structure but also the thermodynamic potential of the system. This induces an indirect exchange interaction between the magnetic layers that can be considered in terms of an effective exchange bias field. The analysis clearly indicates a strong dependence of the effective exchange bias on the properties of the mediating layer, revealing an effective mechanism of electrical control even at room temperature. This dependence also results in qualitatively different characteristics for the cases involving mono- and bilayer graphene.

PACS numbers: 75.70.Cn, 75.80.+q, 75.75.+a, 73.21.Ac

The exchange bias is a phenomenon associated with the unidirectional anisotropy of the exchange interaction at the interface of ferromagnetic (FM) and antiferromagnetic (AFM) materials [1]. Widely used in the magnetic sensors, magnetic random access memory, read heads of hard disk drives, etc., its most important characteristic is the exchange bias field that shifts the centrum of the hysteresis loop. Observation of this phenomenon has generally been attributed to the use of compounds whose FM component has a Curie temperature higher than the Neel temperature of the AFM counterpart. Hence the structure, when cooled in the presence of an external magnetic field, first aligns the FM layer which in turn orders the AFM component accordingly. In the proximity of an AFM pinning layer at or below the Neel temperature, the FM material thus experiences the unidirectional anisotropy induced by the exchange interaction. The temperature dependence can also lead to the unusual effect of spontaneous magnetization reversal through an interplay between the external magnetic field and the exchange bias field aligned in the antiparallel direction [2]. In some cases, the exchange bias field may degrade gradually after multiple recycling of the system through the consequential hysteresis loops (i.e., the so-called training effect in the polycrystalline magnetic materials) [1, 3, 4].

As all the properties described above are related to the magnetic phenomena or the magnetic field repercussion, it raises a natural question: Can an electric field control the exchange bias field at the magnetic interfaces? One potential solution may be to utilize the multiferroic films in place of the FM layers as it has been discussed recently in Ref. [5]. However, the variety of multiferroic materials that can operate at room temperature have so far been limited [5, 6]. On the other hand, a completely different approach may be possible by exploiting the unique properties of atomically thin graphite (i.e., graphene) when placed at the interface between two magnetic dielectric layers. Previous analyses demonstrated that the novel phenomena induced by the exchange interaction between FM layers and monolayer graphene (MLG) [7, 8] or bilayer graphene (BLG) [9] depend sensitively on the detailed electronic features. It certainly offers a ground to explore electrical control of the magnetic interactions, for which the graphene electrons play a vital role.

In this work, we explore the exchange interaction of dielectric magnetic layers mediated by graphene and its manipulation by electrical control. Our theoretical result clearly illustrates that this interaction can be expressed in terms of the effective exchange bias field. It also reveals that the strength of the effective bias field depends critically on the electronic

properties of graphene, particularly the position of the electro-chemical potential (i.e., the carrier density), are amenable for electrical control [10]. Numerical estimates of the predicted phenomenon are provided for an order of magnitude analysis, illustrating its potential significance in spintronic applications.

For accurate understanding, it is useful to identify the underlying differences between those involving MLG and BLG. In the case of MLG, the electron spins polarized by one FM layer interact with the other FM layer mediating their parallel alignment. Therewith the indirect interaction between FM layers amplifies with an increase in the electron density in MLG. On the other hand, the two carbon layers in BLG interact primarily with the nearest magnetic dielectric, respectively, leading to the possibility of inter-layer symmetry break through nonidentical exchange interactions [9]. For example, the difference in the interaction can be achieved by varying the mutual orientation of FM layers that are in contact with BLG at the top and bottom interfaces. In addition to the modified BLG band structure as discussed in Ref. [9] (similar to the case of an external electrical bias [11, 12, 13, 14, 15]), the impact of this asymmetry is more fundamental by energetically favoring an antiparallel configuration in the magnetization orientation of two magnetic layers [16]. Hence, both MLG and BLG can be considered as mediating the exchange interaction (and, thus, the exchange bias) between FM layers, each with a different preference for the bias field orientation.

We begin with a brief analysis of the graphene electronic band structure sandwiched between two magnetic dielectrics. The magnetization belonging to each dielectrics, or more precisely to the proximate strata of FM (or AFM) Im s in contact with graphene [17], is denoted as M_1 and M_2 , respectively. A particularly interesting feature appears for ferromagnetic dielectric layers (FDLs) with an identical magnitude of the magnetic moments ($|M_1| = |M_2| = M$) so that the total magnetization can be varied from zero to $2M$. If the absence of electrically induced asymmetry is further assumed, then only the relative misalignment of M_1 and M_2 provides the cause of symmetry break between two graphene layers in the case of BLG.

Figure 1 schematically illustrates the specific structure under consideration. It resembles the ferromagnet-metal-ferromagnet hybrid structures that reveal a giant magnetoresistance owing to the spin-dependent in-plane conductivity [18]. In our case, graphene substitutes the metallic Im . The magnetization M_1 of the bottom FDL is assumed to be pinned along the x direction by an AFM substrate with a sufficiently strong exchange bias field. The top

FDL is constructed from the same material but its magnetization vector M_2 can be rotated in the x-y plane (by an external or "internal" magnetic field) forming an angle θ with M_1 .

The influence of the FDL magnetization on the graphene electronic structure can be realized in actual structures through either the exchange interaction with magnetic ions (assuming an overlap between the carbon p -orbitals and unfilled shells of the magnetic ions in the FDLs) or an interaction via the ligands of FDLs. Thus, the problem can be modeled in the mean field approximation [7, 8] with the Hamiltonian

$$H^{(n)} = H_G^{(n)} + H_{\text{ex}}^{(n)}; \quad (1)$$

where $H_G^{(n)}$ is the spin-independent MLG ($n = 1$) or BLG ($n = 2$) Hamiltonian. The remaining term of Eq. (1) describes the energy of an electron spin S in the effective fields (in units of energy) M_1 and M_2 of the proximate FDLs, where parameter J is proportional to the carrier-ion exchange constants as evaluated in Refs. [7] and [8]. Hence, it can be written for MLG as

$$H_{\text{ex}}^{(1)} = (M_1 + M_2)S; \quad (2)$$

while the corresponding expression for BLG is

$$H_{\text{ex}}^{(2)} = P_1 M_1 S + P_2 M_2 S; \quad (3)$$

In Eq. (3), the projection operator P_1 (P_2) is 1 for the electron localized at the bottom (top) carbon monolayer and 0 otherwise.

In the case of low energy electronic excitations, the tight-binding approximation accurately describes the band spectra of graphene in the vicinities of each valley K and K^0 [12, 19]. Hence, we adopt the tight-binding Hamiltonian near the valley extrema augmented to account for the electron exchange energy in the form of Eq. (2) or Eq. (3). The qualitative difference between the two spin Hamiltonians [i.e., Eqs. (2) and (3)] implies that $H_{\text{ex}}^{(1)} = 2M \cos(\theta) S_M$ (S_M is the electron spin projection on the direction of sum $M_1 + M_2$) commutes with $H_G^{(1)}$ while this is not the case for $H_{\text{ex}}^{(2)}$ and $H_G^{(2)}$. As a result, MLG remains gapless with four non-degenerate branches $\epsilon_{b,\tau}^{(1)}(k)$ near the K and K^0 points (except the case of $\theta = 0$ that corresponds to $H_{\text{ex}}^{(1)} = 0$). They are identical for the conduction ($b = +1$) and valence ($b = -1$) bands (i.e., the reflection symmetry about $\theta = 0$) and isotropic with respect to the valley centrum $k = 0$. The degeneracy of spin doublet is lifted

as stated, which leads to the expression

$$\epsilon_{b_i}^{(1)}(\mathbf{k}) = b_i v_F k + M \cos \frac{\theta}{2} : \quad (4)$$

Here, $v_F = 10^8$ cm/s is the Fermi velocity in MLG, the subband index $i = 1$, and θ is the angle between \mathbf{M}_1 and \mathbf{M}_2 (0). The impact of the spin Hamiltonian on the MLG band structure is clearly illustrated in Figs. 2 (a) and 2 (b) for two opposite cases of $\mathbf{M}_1/\mathbf{M}_2$ alignment. An important point to note is that, while MLG remains gapless independent of θ and \mathbf{M} following the qualitative discussion given above, the contact (i.e., zero gap) points are shifted to the circle of radius $k_c = (j \mathbf{M} = v_F) \cos \frac{\theta}{2}$ in the k_x - k_y plane (measured from the centrum of the K or K^0 point). Once $\theta = \pi$ and $\mathbf{M}_1 + \mathbf{M}_2$ becomes zero in Eq. (2), the band structure returns to that of unaltered MLG as shown in Fig. 2 (b). Consequently, the density of states for MLG interacting with FM layers modifies to

$$\rho^{(1)}(\epsilon) = 2 \frac{\max_{\mathbf{k}} |\epsilon_{b_i}^{(1)}(\mathbf{k}) - j \mathbf{M} \cos \frac{\theta}{2}|}{\pi v_F^2} ; \quad (5)$$

that is non-zero even at $\epsilon = 0$.

For BLG with the Hamiltonian $H^{(2)}$, a qualitatively different situation is realized due to the interlayer electron transitions with the corresponding matrix element $t_1 = 0.4$ eV. Following the approach discussed in Ref. [9], the BLG energy spectra can be obtained in terms of eight energy branches $\epsilon_{b_i}^{(2)}(\mathbf{k})$ for each valley. Along with band described above, an additional index $i = 1$ is introduced to distinguish four low-energy bands $\epsilon_{b_i}^{(2)}(\mathbf{k})$ from the other four excited states with energies $\epsilon_{b_i+1}^{(2)}(\mathbf{k})$ & $\epsilon_{b_i-1}^{(2)}(\mathbf{k})$. As it is convenient to normalize the parameters in units of t_1 , the dimensionless momentum $p = v_F k = t_1$ and the effective field $G = M/t_1$ are used hereinafter. Then, the energy bands can be expressed as

$$\epsilon_{b_i}^{(2)}(p) = b_i \sqrt{p^2 + \frac{G^2}{4} + \frac{1}{2}} \pm G \cos \frac{\theta}{2} + W_{\pm}(p) ; \quad (6)$$

where

$$W_{\pm}(p) = \frac{1}{2} \sqrt{1 + G^2 \cos^2 \frac{\theta}{2} + 4p^2} \pm p G \sin \frac{\theta}{2} : \quad (7)$$

Four solutions with $\epsilon_{b_i+1}^{(2)} > 0$ correspond to the conduction bands, while their mirror images with respect to the zero energy describe the highest valence bands ($b = -1$).

In contrast to MLG, the calculation clearly illustrates the presence of an energy gap ϵ_g between the lowest conduction band and the highest valence band as soon as $\theta \neq 0$.

When the orientation of M_1 and M_2 is in a parallel alignment ($\theta = 0$), the net effect of the exchange interaction simply lifts the two-fold spin degeneracy resulting in two pairs of spin-split bands that cross each other at $p = \frac{P}{G(1+G^2)=2}$ as shown in Fig. 2(c). However, once they are misaligned, the electronic bands become of mixed spin character (e.g., with both parallel and antiparallel components to the x direction). Subsequent anti-crossing opens up the gap that progressively grows with θ . At $\theta = \pi$ in Fig. 2(d) (i.e., $M_1 = -M_2$), the gap reaches the maximum while the energy bands regain the two-fold degeneracy similar to MLG [9]. Accordingly, the BLG density of states $\rho^{(2)}(\epsilon)$ is zero for $|\epsilon| > \epsilon_g/2$, where $\epsilon_g = \frac{1}{2}G \sin^2 \frac{\theta}{2} = \frac{1}{2}(1 + G^2 + 2G \cos \frac{\theta}{2})$. As the density of states determines the characteristic carrier occupancy, the calculation result strongly indicates that the total electronic energy of the structure can be controlled by the orientation of M_1 and M_2 or, more specifically, by the angle θ . This point is schematically illustrated in Fig. 2 through the comparison of shaded regions representing the occupied states when the electro-chemical potential (dashed line) is hypothetically located at $\epsilon = 0$.

Now we can take into account the entropy effects at finite temperature along with the band modification [Eqs. (4) and (6)] by evaluating the thermodynamic potential

$$\Omega^{(n)}(\epsilon) = -2k_B T \sum_{\text{fm g}} \sum_{\mathbf{k}} \ln \left[1 + \exp \left(-\frac{\epsilon_{\text{fm g}}^{(n)}(\mathbf{k})}{k_B T} \right) \right]; \quad (8)$$

where k_B is the Boltzmann constant, T is the temperature, $n = 1; 2$ denotes the cases of MLG and BLG, respectively, and fm g collectively represents the band indices described earlier. Additionally, the factor of 2 comes from the summation over the valleys K and K^0 . One remarkable outcome from the calculations of thermodynamic potential [Eq. (8)] is the universal scalability of the dependence on angle θ for both MLG and BLG:

$$\frac{\Omega^{(n)}(\epsilon)}{\Omega^{(n)}(0)} = \frac{1}{2} (1 - \cos \theta); \quad (9)$$

where $\Omega^{(n)}(\epsilon) = \Omega^{(n)}(\epsilon) - \Omega^{(n)}(0)$. In other words, the relative change in the thermodynamic potential [Eq. (9)] is independent of all parameters except $\cos \theta$ in spite of its seemingly complex expression [see Eqs. (4), (6), and (8)].

Clearly, Eq. (9) indicates that the free energy of the system either increases or decreases as the magnetization of the free FDL (M_2) rotates from the parallel ($\theta = 0$) to the antiparallel ($\theta = \pi$). Since a lower free energy is favored, it means that M_2 is inclined to take one of the orientations depending on the sign of $\Omega^{(n)}(\epsilon)$. This preference on the magnetization

orientation can also be described in terms of the magnetic energy of the FM layer when it is subject to a magnetic field: i.e., $M(\theta) = H_{\text{eb}} M_2 = H_{\text{eb}} M_2 \cos \theta$, where the x axis is chosen as the reference direction for the magnetic field and $M_2 = M_2 A_0 t_F$ is the total magnetic moment of the top FDL with A_0 and t_F its area and thickness. Through comparison with Eq. (9), one can readily deduce the strength of the effective magnetic field $H_{\text{eb}}^{(n)}$ that is essentially the exchange bias field mediated by graphene,

$$H_{\text{eb}}^{(n)} = \frac{n(\theta)}{2M_2} : \quad (10)$$

As in the case of conventional exchange bias, the strength of $H_{\text{eb}}^{(n)}$ is inversely proportional to the thickness t_F [1]. However, one distinguishing feature of the exchange bias field given in Eq. (10) is its dependence on the electronic properties of the graphene layer, particularly the position of the electro-chemical potential that can be readily modulated by the gate bias (V_{g1}, V_{g2} ; see Fig. 1). This also leads to qualitatively different characteristics for MLG and BLG that the calculation of $n(\theta)$ highlights.

Firstly, the signs of $H_{\text{eb}}^{(1)}$ and $H_{\text{eb}}^{(2)}$ are different at least in the range $j \in [0, 3]$. While MLG tends to establish M_2 parallel to M_1 ($H_{\text{eb}}^{(1)} > 0$), BLG favors the antiparallel alignment ($H_{\text{eb}}^{(2)} < 0$) as pointed out in our discussion earlier. Secondly, a shift of μ from the graphene charge neutrality point ($\mu = 0$) affects the strengths of the exchange bias fields in the opposite directions. Namely, the magnitude of $H_{\text{eb}}^{(1)}$ gradually increases with j whereas that of $H_{\text{eb}}^{(2)}$ is at the maximum at $\mu = 0$ and decreases to zero. A similar pattern is also observed in the temperature dependence. As T goes up, $H_{\text{eb}}^{(1)}$ becomes stronger and $H_{\text{eb}}^{(2)}$ weaker when μ is at or around the graphene charge neutrality point. The properties of $H_{\text{eb}}^{(1)}$ can be readily explained by considering the concentration variation of the conduction electrons and valence holes that can be spin polarized and therefore establish an effective field affecting equally the bottom and top FM layers. Hence, the parallel alignment of two ferromagnets are energetically favored and the magnitude of the indirect exchange bias field increases with the mediating carrier density (i.e., j) when MLG is used. On the other hand, the effect of $H_{\text{eb}}^{(2)}$ can be thought in terms of the band structure modification such as the size of the gap. As a larger gap pushes the energies of the occupied states lower, the thermodynamic potential decreases likewise. This prefers a larger angle θ with $H_{\text{eb}}^{(2)} < 0$ (i.e., antiparallel). Increasing j and T diminishes the effect and, thus, the magnitude of $H_{\text{eb}}^{(2)}$.

The aforementioned characteristics can be captured by an approximate expression in the limit of small G ,

$$J_n(\mu) \approx N G^2 f_n(\mu; T); \quad (11)$$

where N is the number of graphene primitive cells at the interface and the factor $f_n(\mu; T)$ provides the specific dependence on μ and T for MLG ($n = 1$) and BLG ($n = 2$). The dependence of the exchange bias field [Eqs. (10) and (11)] on the square of the effective field G is not surprising as the indirect interaction between the bottom (M_1) and the top (M_2) ferromagnets involves two interfaces with graphene. Figure 3 shows $f_n(\mu; T)$ vs. μ evaluated at three different temperatures. As expected, the temperature factor has a considerable influence around $\mu = 0$ but its role diminishes significantly for $|\mu| > 0.2 \text{ eV}$ ($\mu = 0.4 \text{ eV}$). More crucial is the possibility of controlling $f_n(\mu; T)$ (thus, $H_{\text{eb}}^{(n)}$) over a wide range even at room temperature. As evident from the figure, the shift of $\mu \approx 0.15 \text{ eV}$ can change the strength of $H_{\text{eb}}^{(n)}$ by about a factor of two for both cases mediated by MLG and BLG. Based on these results, a rough estimate can be made for the magnitude of $H_{\text{eb}}^{(n)}$. Assuming $|f_n| \approx 1 \text{ meV}$ (a typical number from Fig. 3) [20], a high temperature FM dielectric such as yttrium iron garnet, and $G = 0.1$ for the graphene interface ($\mu G = 40 \text{ meV}$) [9], one can find $t_{\text{FM}} H_{\text{eb}}^{(n)} \approx 1100 \text{ Oe}$, where t_{FM} is the FM layer thickness in nm (e.g., $H_{\text{eb}}^{(n)} \approx 1100 \text{ Oe}$ at $t_{\text{FM}} = 1 \text{ nm}$). Electrical control of the exchange bias in the estimated range can be of practical importance in a number of spintronic applications.

In summary, our theoretical analysis shows that graphene can mediate the indirect interaction of magnetic layers resulting in an effective exchange bias. Through the dependence on the graphene electro-chemical potential, it is also clearly identified that the effective exchange bias can be modulated electrically over a wide range even at room temperature. The numerical estimation indicates the potential significance of the proposed phenomenon in practical applications.

This work was supported in part by the US Army Research Office and the FC/RP Center on Functional Engineered Nano Architectonics (FENA).

-
- [1] J. Nogues and I. K. Schuller, *J. Magn. Mater.* **192**, 203 (1999).
- [2] Z. P. Li et al., *Phys. Rev. Lett.* **96**, 137201 (2006).
- [3] K. Zhang, T. Zhao, and M. Fujiwara, *J. Appl. Phys.* **89**, 6010 (2001).
- [4] A. Hochstrat, Ch. Binek, and W. Kleemann, *Phys. Rev. B* **66**, 092409 (2002).
- [5] H. Bea et al., *Phys. Rev. Lett.* **100**, 017204 (2008).
- [6] C.-G. Duan et al., *Phys. Rev. Lett.* **97**, 047201 (2006).
- [7] Y. G. Semenov, K. W. Kim, and J. Zavada, *Appl. Phys. Lett.* **91**, 153105 (2007).
- [8] H. Haugen, D. Huertas-Hemando, and A. Brataas, *Phys. Rev. B* **77**, 115406 (2008).
- [9] Y. G. Semenov, J. M. Zavada, and K. W. Kim, *Phys. Rev. B* **77**, 235415 (2008).
- [10] A. K. Geim and K. S. Novoselov, *Nat. Mater.* **6**, 183 (2007).
- [11] K. S. Novoselov et al., *Nat. Phys.* **2**, 177 (2006).
- [12] E. McCann and V. I. Fal'ko, *Phys. Rev. Lett.* **96**, 086805 (2006).
- [13] E. V. Castro et al., *Phys. Rev. Lett.* **99**, 216802 (2007).
- [14] H. Min et al., *Phys. Rev. B* **75**, 155115 (2007).
- [15] E. McCann, D. S. L. Abergel, and V. I. Fal'ko, *Eur. Phys. J. Spec. Top.* **148**, 91 (2007).
- [16] Note that the prospective effect is in accordance with other physical phenomena (such as the Jahn-Teller effect, Peierls transition, etc.) of electronic stabilization through the spontaneously broken symmetry.
- [17] W. H. Micklejohn and C. P. Bean, *Phys. Rev.* **105**, 904 (1957).
- [18] See, for example, M. N. Babich et al., *Phys. Rev. Lett.* **61**, 2472 (1988).
- [19] J. C. Slonczewski and P. R. Weiss, *Phys. Rev.* **109**, 272 (1958).
- [20] An interlayer exchange coupling of the same order of magnitude was found for Fe-Fe through MgO. See T. Katayama et al., *Appl. Phys. Lett.* **89**, 112503 (2006).

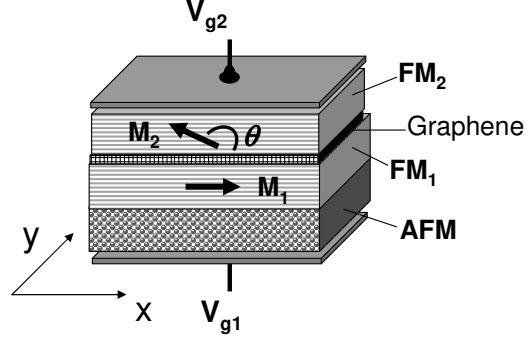


FIG .1: Schematic illustration of graphene sandwiched between two FM dielectric layers FM_1 and FM_2 of magnetization M_1 and M_2 . While M_1 is pinned by an AFM layer along the x direction, M_2 can rotate on the x-y plane with specifying the angle between them. The structure can be placed between metallic contacts providing electrical control with the gate voltages V_{g1} and V_{g2} .

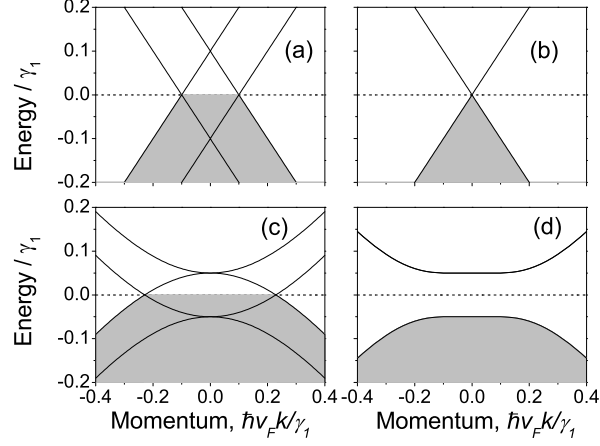


FIG. 2: Energy band diagram of (a,b) mono- and (c,d) bilayer graphene when sandwiched between two FM materials as shown in Fig. 1. For (a) and (c), the angle between M_1 and M_2 is zero (i.e., parallel alignment) and no gap exists between the bands. In the cases of (b) and (d), $\theta = \pi$ (antiparallel) and the bands are doubly degenerate. The shaded regions schematically represent the occupied valence bands with $\mu = 0$ (dashed line) at $T = 0$. The effective field $G = 0.1$ is assumed for the calculation and the momentum is measured from the K or K^0 valley centrum. $\gamma_1 = 0.4$ eV and $v_F = 10^8$ cm/s.

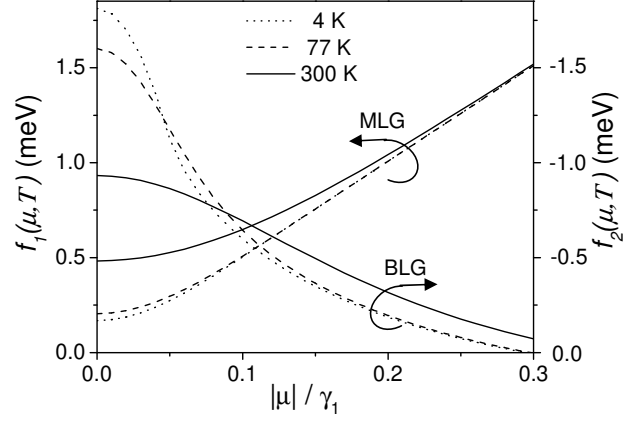


FIG. 3: Factor $f_n(\mu, T)$ [$f_n(\mu, T) = N G^2$] vs. $|\mu|/\gamma_1$ evaluated at three different temperatures ($n = 1$ for MLG; $n = 2$ for BLG). This factor essentially determines the dependence of exchange bias field on μ and T .